SANDIA REPORT
SAND2007-3930
Unclassified Unlimited Release
Printed June 2007

Radial Electric Field 3D Modeling for Wire Arrays Driving Dynamic Hohlraums on Z

Raymond C. Mock

Prepared by
Sandia National Laboratories
Albuquerque, New Mexico 87185 and Livermore, California 94550

Sandia is a multiprogram laboratory operated by Sandia Corporation,
a Lockheed Martin Company, for the United States Department of Energy's
National Nuclear Security Administration under Contract DE-AC04-94AL85000.

Issued by Sandia National Laboratories, operated for the United States Department of Energy by Sandia Corporation.

Available to DOE and DOE contractors from
U.S. Department of Energy
Office of Scientific and Technical Information
P.O. Box 62
Oak Ridge, TN 37831

Telephone: (865) 576-8401
Facsimile: (865) 576-5728
E-Mail: reports@adonis.osti.gov
Online ordering: http://www.osti.gov/bridge

Available to the public from
U.S. Department of Commerce
National Technical Information Service
5285 Port Royal Rd.
Springfield, VA 22161

Telephone: (800) 553-6847
Facsimile: (703) 605-6900
E-Mail: orders@ntis.fedworld.gov
Online order: http://www.ntis.gov/help/ordermethods.asp?loc=7-4-0#online

SAND2007-3930
Unclassified Unlimited Release
Printed June 2007

Radial Electric Field 3D Modeling for Wire Arrays Driving Dynamic Hohlraums on Z

Raymond C. Mock*
Diagnostics & Target Physics Department
Sandia National Laboratories
P.O. Box 5800
Albuquerque, NM 87185-0958

Abstract

The anode-cathode structure of the Z-machine wire array results in a higher negative radial electric field (E_r) on the wires near the cathode relative to the anode. The magnitude of this field has been shown to anti-correlate with the axial radiation top/bottom symmetry in the DH (Dynamic Hohlraum). Using 3D modeling, the structure of this field is revealed for different wire-array configurations and for progressive mechanical alterations, providing insight for minimizing the negative E_r on the wire array in the anode-to-cathode region of the DH. Also, the 3D model is compared to Sasorov's approximation, which describes E_r at the surface of the wire in terms of wire-array parameters.

* Contractor for Ktech Corporation, 10800 Gibson, SE, Albuquerque, NM 87123

Acknowledgements

Thanks to the following collaborators: T. W. L. Sanford, R. J. Leeper, and J. L. Porter for program support, T. J. Nash and W. A. Stygar for technical support, L. F. Bennett and D. L. Smith for 3D model assistance, D. G. Schroen for hardware photographic and measurement assistance, D. H. Romero for hardware discussions, and T. J. Nash, M. E. Cuneo, and L. F. Bennett for carefully revising this report.

Table of Contents

I. INTRODUCTION

The Z-machine load z-pinches a tungsten wire array onto a central low-density foam target (Figure 1A) to produce a dynamic-hohlraum (DH) [1-4], an intense blackbody x-ray source, for inertial-confinement-fusion [5-9] and high-temperature radiation flow experiments [10-11].

The axial radiation top/bottom symmetry in the DH has been shown to anti-correlate with the magnitude of the negative radial electric field (E_r in Figure 1A) at the wire [12, 13] (outside wire for nested arrays) given by Sasorov's approximation (Figure 1B) [14]. The influence of the radial electric field on the wire pinch is illustrated in Figure 2 and is described as follows. At very early times, E_r (Figure 2A) affects the axial current distribution by enhancing electron emission from the wire and generating early breakdown of the vapor surrounding the wire (Figure 2B). The current shunts to the resulting coronal plasma rather than remaining in the core. The wire core remains cold near the cathode creating a energy deposition imbalance between the top and bottom of the z-pinch, resulting in an axial radiation asymmetry at stagnation.

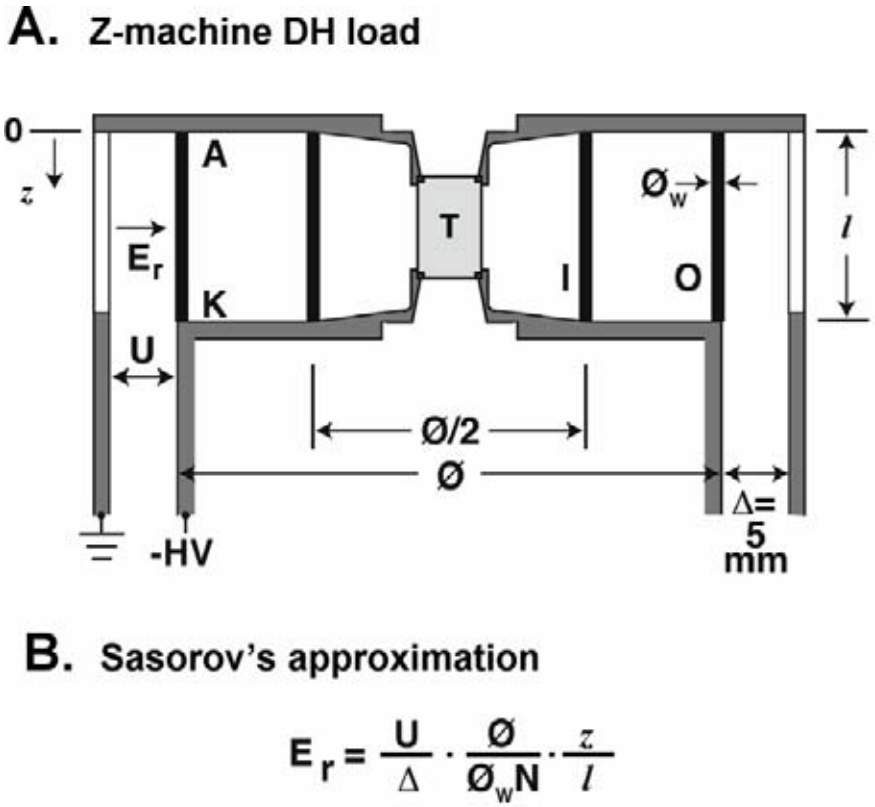

Figure 1. (A) the z-machine load consisting of drive potential U in AK gap Δ, inner (I) and outer (O) wire arrays of wire diameter $Ø_w$, AK region of height *l*, Target (T), and negative radial electric field (E_r) acting on outer wire array. (B) Sasorov's approximation where N is the number of outer wires and *z* is zero at the anode.

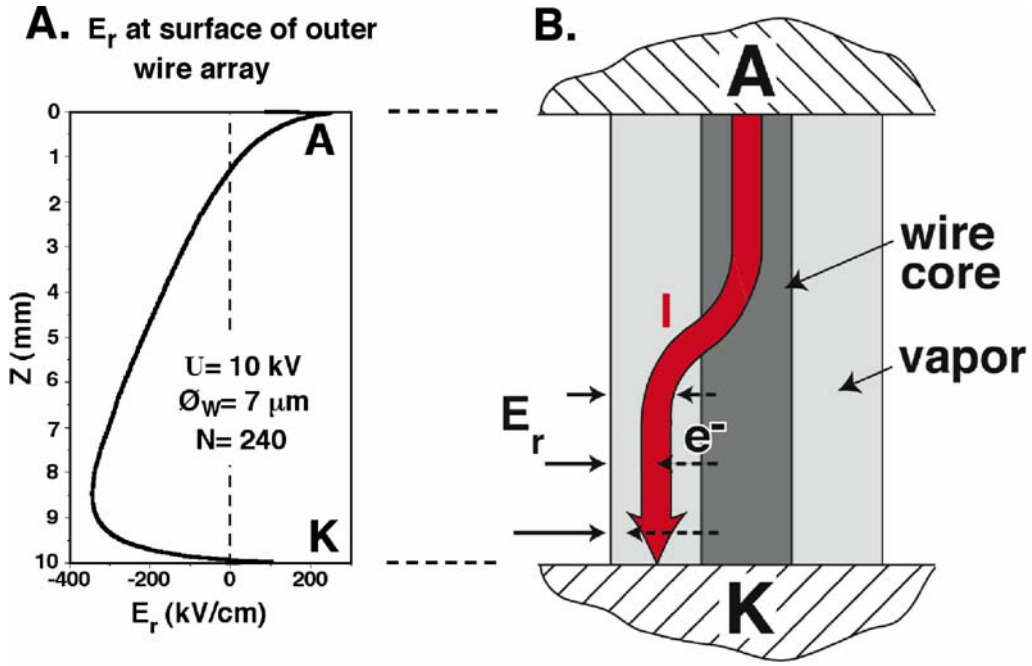

Figure 2. (A) 3D model of radial electric field E_r at z in AK region. (B) Illustration of E_r effect on wire-core electrons and current path.

A 3D model is used to evaluate E_r at the wires and look for a means of mitigating its magnitude in critical regions. Section II describes the 3D model. Section III compares the 3D model of E_r at the wire with Sasorov's approximation. Section IV looks at wire fixturing in general. Following sections consider the effect on E_r at the wire with progressive mechanical alterations to provide insight for minimizing the negative electric field on the wire array in the anode-cathode (AK) region: section V looks at the radial electric field with wire variation; section VI, with indented cathode variation; section VII, with an anode wire cavity; and section VIII, with indented AK variation. Note, E_r derivations throughout these sections do not account for interdependence of parameters.

II. THE 3D MODEL

Modeling utilizes Coulomb v6.4 [15], a static 3D electric-field solver and analysis software. A 2D structure is modeled in r-z and swept 1.5° through θ (360°/240-wires) for a $1/240^{th}$ section (Figure 3A). The wire is added on the r-z center-plane of the section. Boundary conditions are set for anode (0 V), cathode (-10000 V), and wire (linear, 0 to -10000 V), and a 240 periodicity is set about z. Material is set for anode and cathode (stainless steel) and wire (tungsten). Discretizing is set at approximately 4000±1000 2D elements but increases for smaller diameter wires (10000 elements for 7 μm wire) balancing structure complexity and run time. A 35 μm wire diameter is generally used in modeling to limit the number of 2D elements and thus limit the run time. The problem is then solved (run) and analyzed with 1D, 2D, or 3D analysis methods.

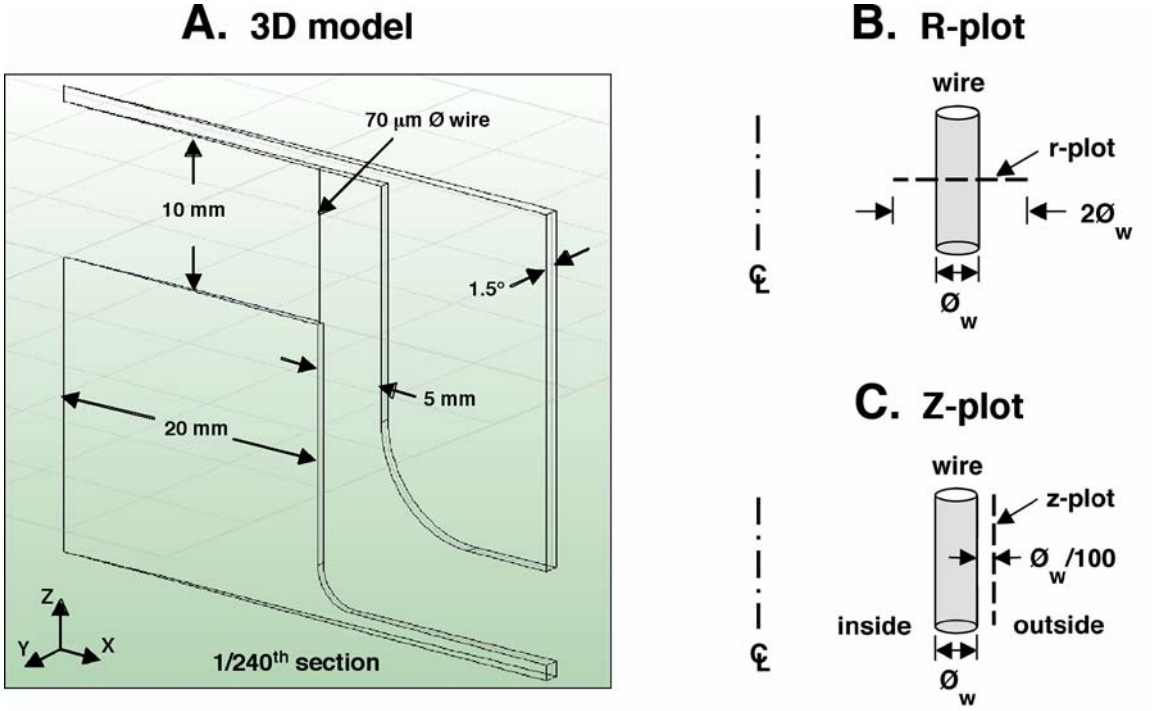

Figure 3. (A) 3D model of 1/240th section. (B) R plot for determining radial electric field E_r at the wire. (C) Z plot for determining E_r along the wire.

Discrete E_r values are derived at the wires using r-plots (Figure 3B) passing radially through and centered on the wire with a length of two times the wire diameter and with 400 data points (dp) giving E_r values accurate to 1.1±0.3 percent. E_r values along the wires, z-plots (Figure 3C), are placed at 1/100 the wire diameter from the wire, radially outside or inside, with 300 to 3000 data points (to be addressed in section V). R-plot and z-plot E_r values are in agreement by 0.15±0.9 percent at nearest crossover points.

III. SASOROV'S APPROXIMATION

Using the 3D model (Figure 4A), the parameters in Figure 4A, and letting *z* equal half of *l* (Figure 4B), the 3D radial electric field is compared with that of Sasorov's approximation for four parameters of the wire array: array diameter Ø, wire diameter $Ø_W$, wire number N, and radial AK gap Δ (Figure 4C-F). At the baseline (except for $Ø_w$) parameters (Ø= 40 mm, $Ø_w$= 35 μm, N= 240, Δ= 5 mm), Sasorov's approximation is normalized 22 percent higher to match the 3D model. E_r tracks to first order, diverging more at the lower variables from eight percent for Δ to 59 percent for N.

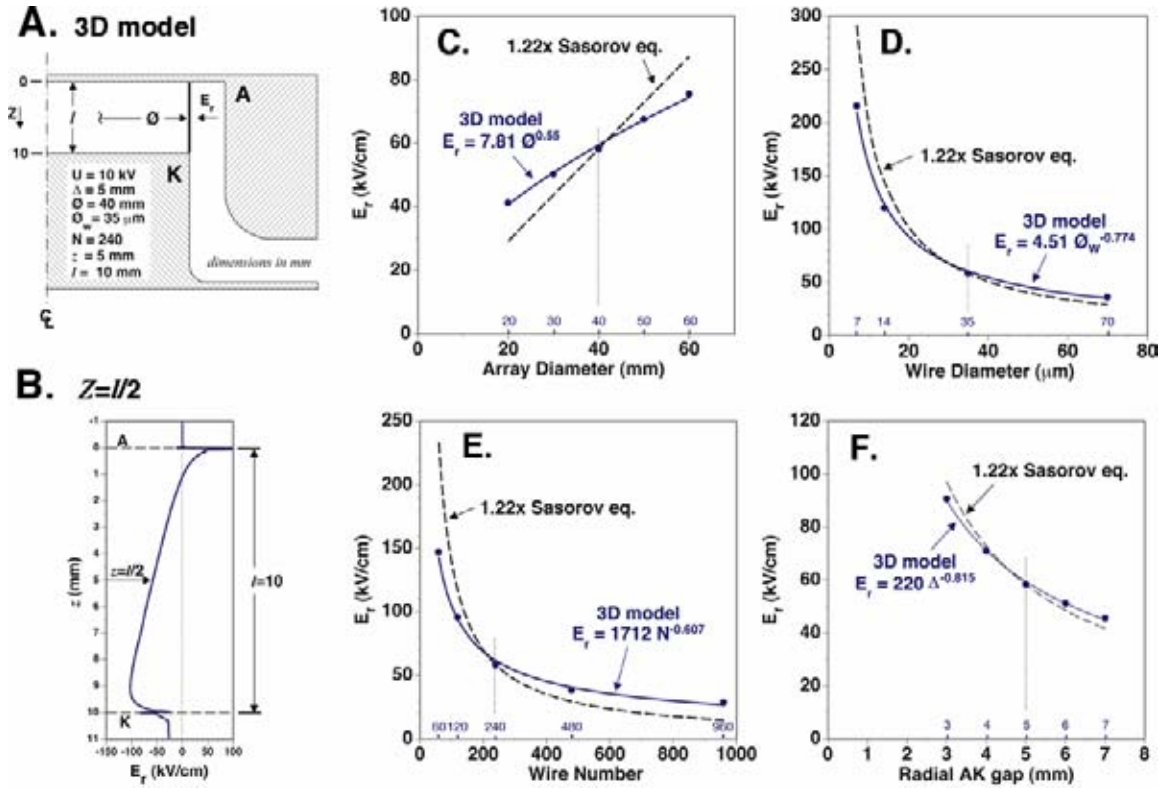

Figure 4. Radial electric field comparison of (A) 3D model and (Fig. 1B) Sasorov's approximation using (A) baseline parameters (except for wire diameter $Ø_w$) at (B) $z = l/2$ and changing (C) array diameter Ø, (D) wire diameter $Ø_w$, (E) wire number N, and (F) radial AK gap Δ.

The parameters in Figure 4A correspond to those of the baseline DH [10,13] with exception of the wire diameter $Ø_W$. Again, the diameter of 35 μm was selected to keep the run time within two hours. The baseline DH wire diameter is 7.5 μm.

IV. WIRE FIXTURING

Figure 5A illustrates a typical fixture for wire arrays [16]. A single wire is drawn across the bottom of the cathode, is passed through a 50-μm wide slot (Figure 5C) with a 45-degree edge (Figure 5B) providing location and current contact at anode and cathode, and is terminated by weight at each end to provide tension. The wire runs 7.4 mm along the cathode radial surface and runs 1.9 mm along the anode radial surface where it also passes through a 125 μm wide cavity (Figure 5B). The hardware design was driven by the need to include an inner wire array and to provide top and bottom viewing. The resulting hardware was then slotted to provide the wire routes. Assembly procedure is also a factor in the design.

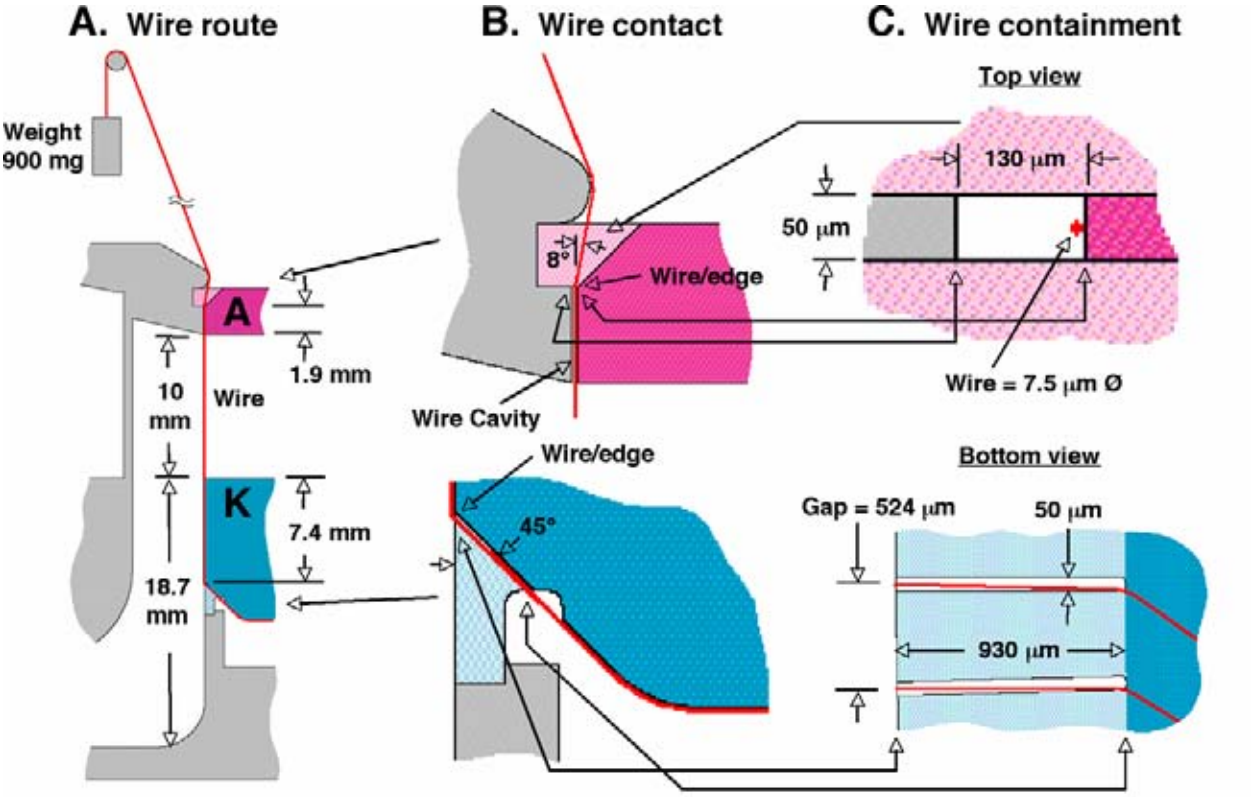

Figure 5. Typical wire array fixture showing (A) wire route, (B) wire contact points, and (C) wire containment slots.

A 7.5 μm diameter wire is shown magnified at the cathode slot (Figure 6B) where it emerges and maintains a distance of 25 to 40 μm from the cathode up to the cathode edge (Figure 6A). A ridge can be seen at the edge of the cathode in close proximity to the wire. This photo illustrates that the wire makes current contact at the lowest point on the wire (the cathode slot). A misalignment of the anode to cathode of 102 μm would lean the wire array making contact at the upper cathode edge and disrupt azimuthal symmetry of the radial electric field. A ridge at the edge would make misalignment proportionately more critical. A Misalignment of 25 μm is standard but it can be as much as 76 μm or more where delicate parts become elliptical with processing and alignment sleeves have to be reduced in diameter.

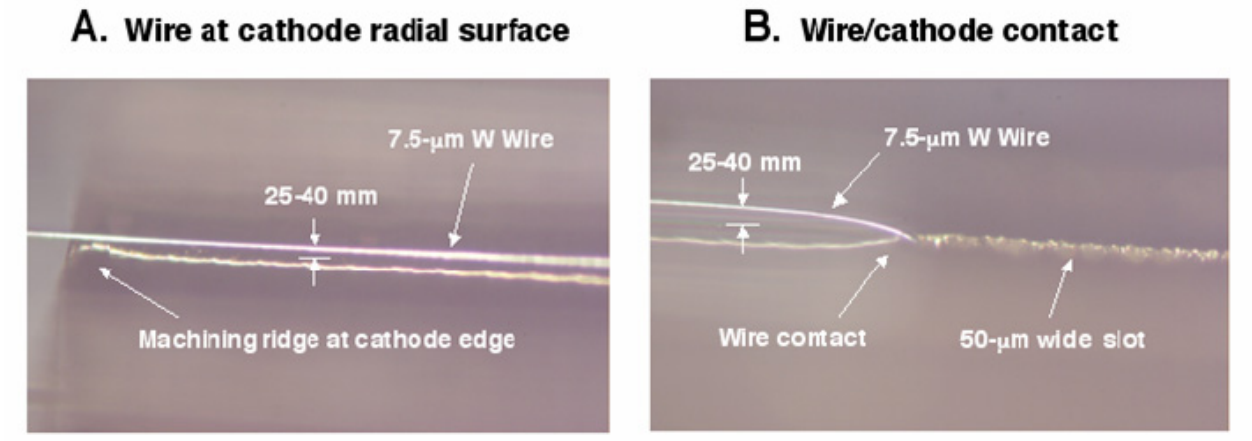

Figure 6. Magnified photo of an array wire along the cathode radial surface (A) at upper edge of cathode and (B) at slot of cathode.

V. WIRE VARIATION

The 3D model is used to derive the radial electric fields for wire placements and lengths (Figure 7A). With a fixed cathode diameter of 40 mm and a fixed 10-mm AK corresponding to the baseline DH [10,13], the wire-array diameter $Ø_A$ is placed at 36, 38, and 40 mm within the 10-mm AK (Figure 7B-D) and at 40.07 mm outside the 10-mm AK where the total suspended wire-array length l_A is 10, 12.5, and 17.5 mm (Figure 7E-G). Wire placement further within the 10-mm AK results in lower radial electric field strength and more A-to-K symmetry. Wire length variation outside the 10-mm AK results in dramatic reversal of radial electric field polarity as close placement of wire to the cathode radial surface provides a positive radial electric field on the wire, greatest near the cathode radial surface upper edge. Wire length variation also provides reversal of the field polarity at the anode end of the wire (Figure 7F, G). Wire length variation has a slight effect on the radial electric field on the wire within the central region of the 10-mm AK (Figure 7E-G).

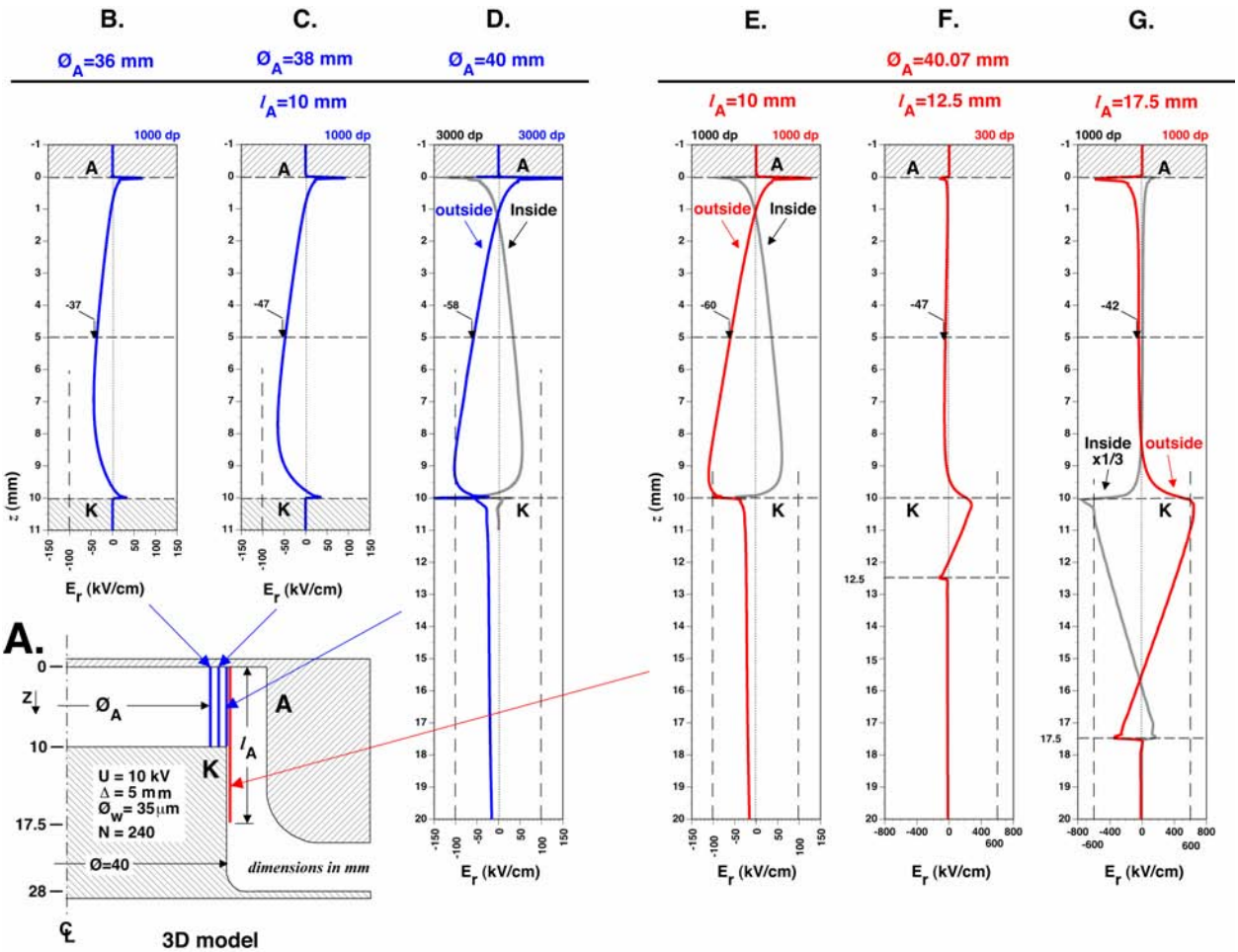

Figure 7. (A) 3D-model for deriving radial electric fields using 35-μm wire for (B-D) wire-array diameters Q_A within the AK and (E-G) suspended wire-array lengths l_A outside the 10-mm AK. The number of data points (dp) per plot are indicated.

Z-plots within the AK start 1 mm below the cathode and end 1 mm above the anode. Z-plots outside the AK start and end with the model geometry. At the wire ends, the electric field spikes to high values. A data point on the high field spike terminates the 3D program, and so the number of data points per z-plot is limited giving a conservative electric field value for these high wire-end field spikes.

VI. INDENTED CATHODE VARIATION

Because a wire inside the AK is geometrically complex (cavities, cavity fields, parts, etc.), because the outside wire provides the tool to reverse the high negative radial electric field near the cathode, and because close placement of the wire to the cathode creates alignment issues, indentation of the cathode is now considered for controlling the positive electric field strength. Figure 8A illustrates the indentation variable I. Figure 7G is duplicated in Figure 8B for a starting point and the indentation is 0, 0.5, and 1 mm (Figure 8B-D). The increasing indent lowers the intensity of the positive radial electric field and nulls the high negative electric field spike at the anode end with 1 mm indentation. The negative radial electric field in the central region of the AK is also reduced (Figure 8B-D).

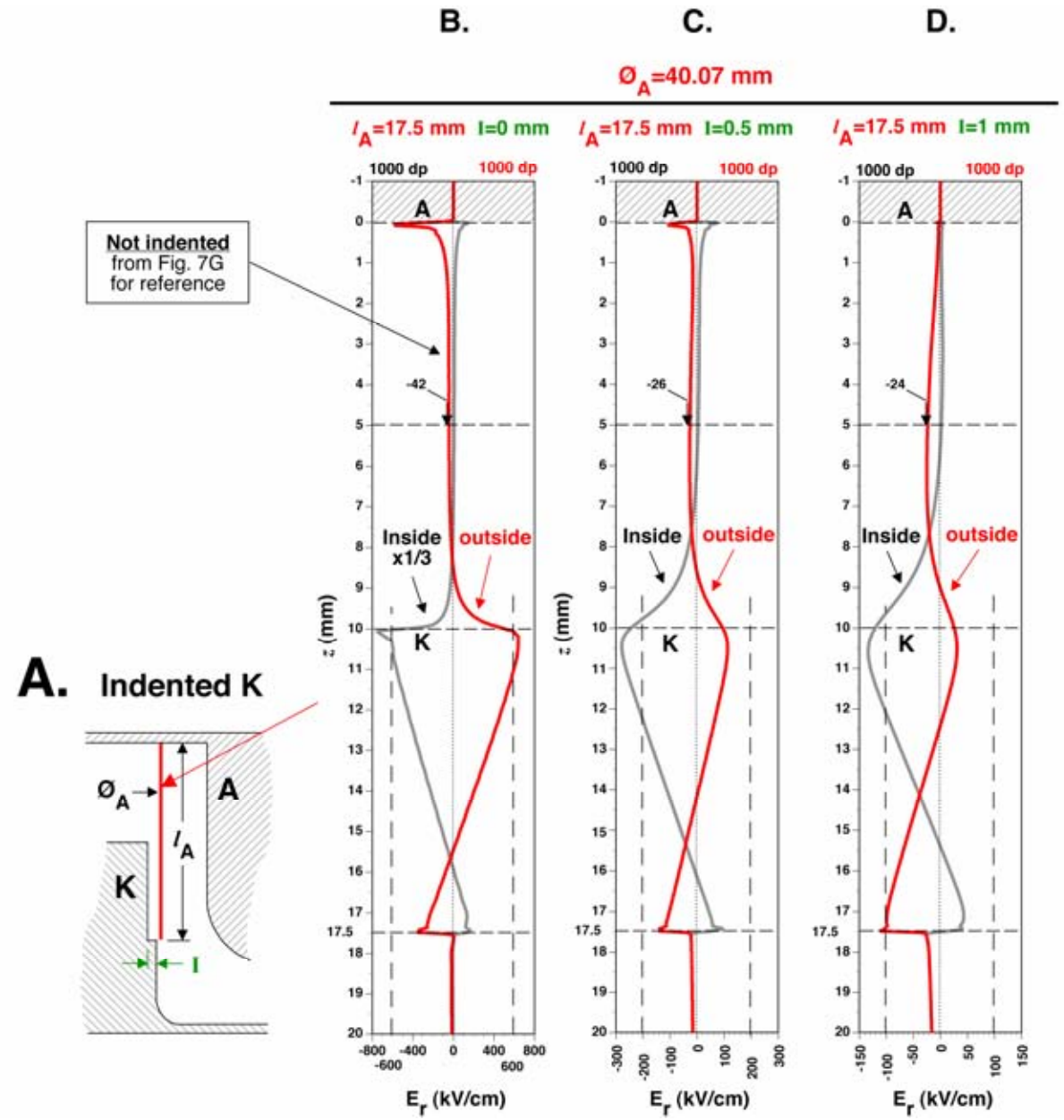

Figure 8. (A) Indented cathode 3D-model for deriving radial electric fields for (B-D) cathode indentation I, using 35-μm wire. B is duplicated from Fig. 7G for reference. The number of data points (dp) per plot are indicated.

VII. ANODE WIRE CAVITY

The wire cavity at the radial surface of the anode is modeled in Figure 9A. As a drastic negative electric field is expected due to the 125 µm width of the cavity, Figure 7E is duplicated in Figure 9B for a starting point. Figure 7C shows the negative radial electric field near the cathode region is now extended to the anode region and exacerbated in the 2-mm AK region near the anode.

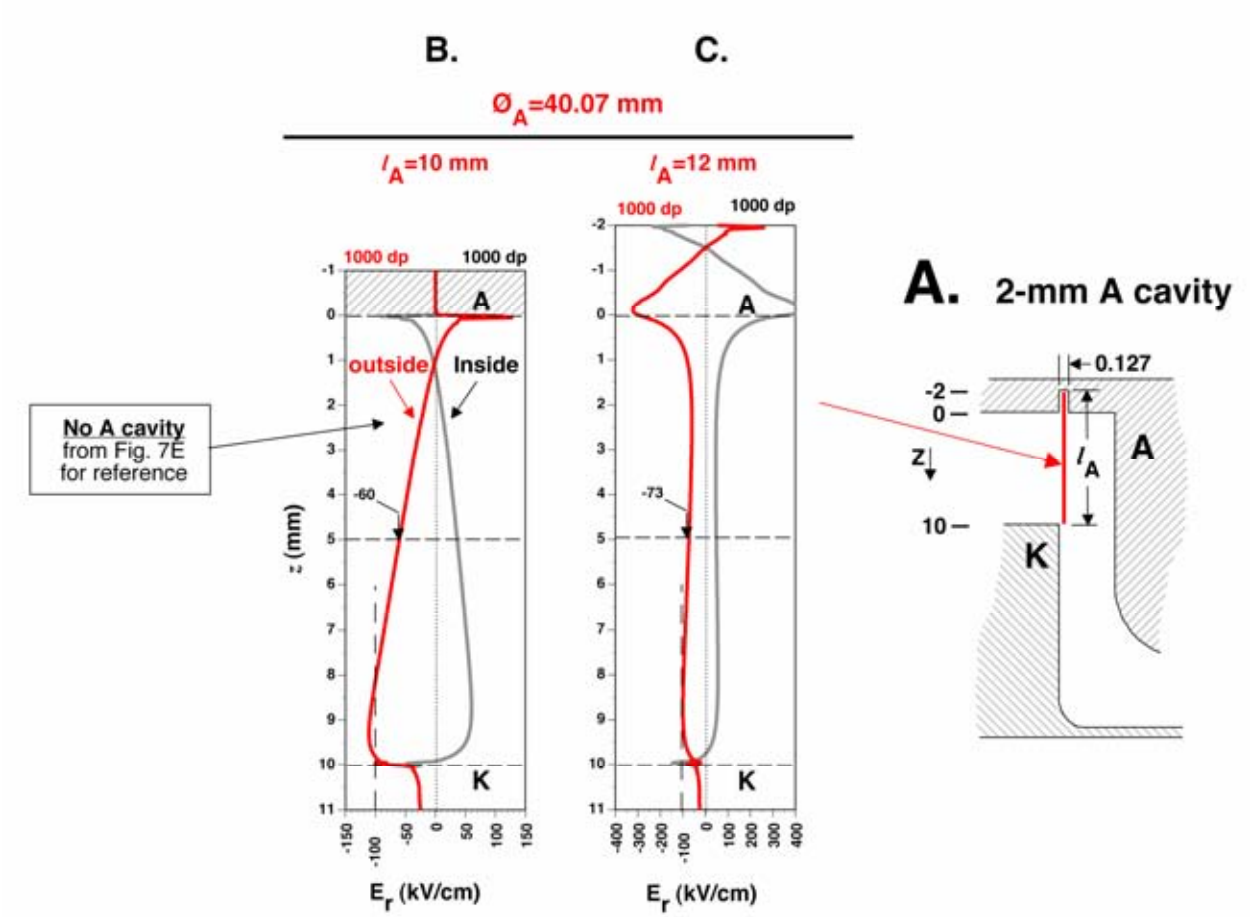

Figure 9. (A) 3D-model for deriving radial electric fields (B) without and (C) with a 2-mm high, 127-µm wide anode cavity, using 35-µm wire. B is duplicated from Fig. 7E for reference. The number of data points (dp) per plot are indicated.

VIII. INDENTED ANODE-CATHODE VARIATION

To lower the anode wire-cavity effect, the anode cavity depth is reduced by cutting material away. A limit is approached as some material must remain to capture the anode wafer on the current return can (Figure 5B). The cavity depth is 1.9 mm (Figure 5A), so 1 mm is removed in the model (Figure 10A, C, D). Figure 8D is duplicated in Figure 10B as a starting point. The anode and cathode are indented equally from 1 to 0.5 mm (Figure 10C, D). The null of Figure 10B is removed by the wire extension of 1 mm in Figure 10C but is over-compensated by the indent reduction in Figure 10D.

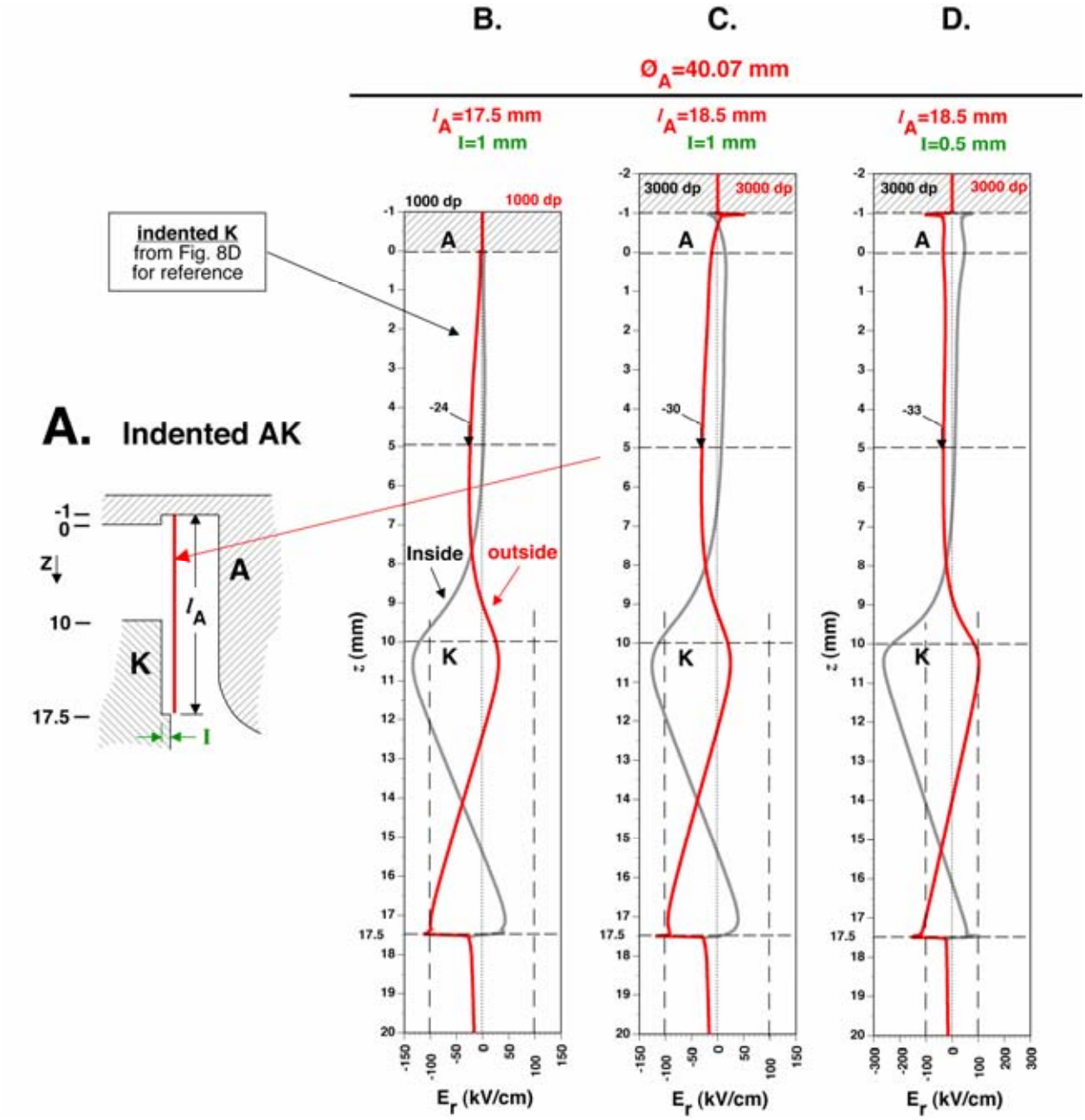

Figure 10. (A) 3D-model for deriving radial electric fields for (B) cathode indentation I and (C, D) AK indentation I, using 35-μm wire. B is duplicated from Fig. 8D for reference. The number of data points (dp) per plot are indicated.

A limited anode cavity of 1 mm is now added in Figure 11A. Figure 10C is duplicated in Figure 11B as a starting point. The anode cavity again exhibits its negative electric field effect extending the negative radial electric field at the cathode region to the anode region, but the exacerbated negative field is now limited to the 1-mm AK region near the anode where the indent exists. Note that the field in Figure 11B may be possible if the 45º anode slot (Figure 5B) were cut further down bringing the wire contact closer to the anode surface of the AK, but plasma may more readily exit through the anode slots.

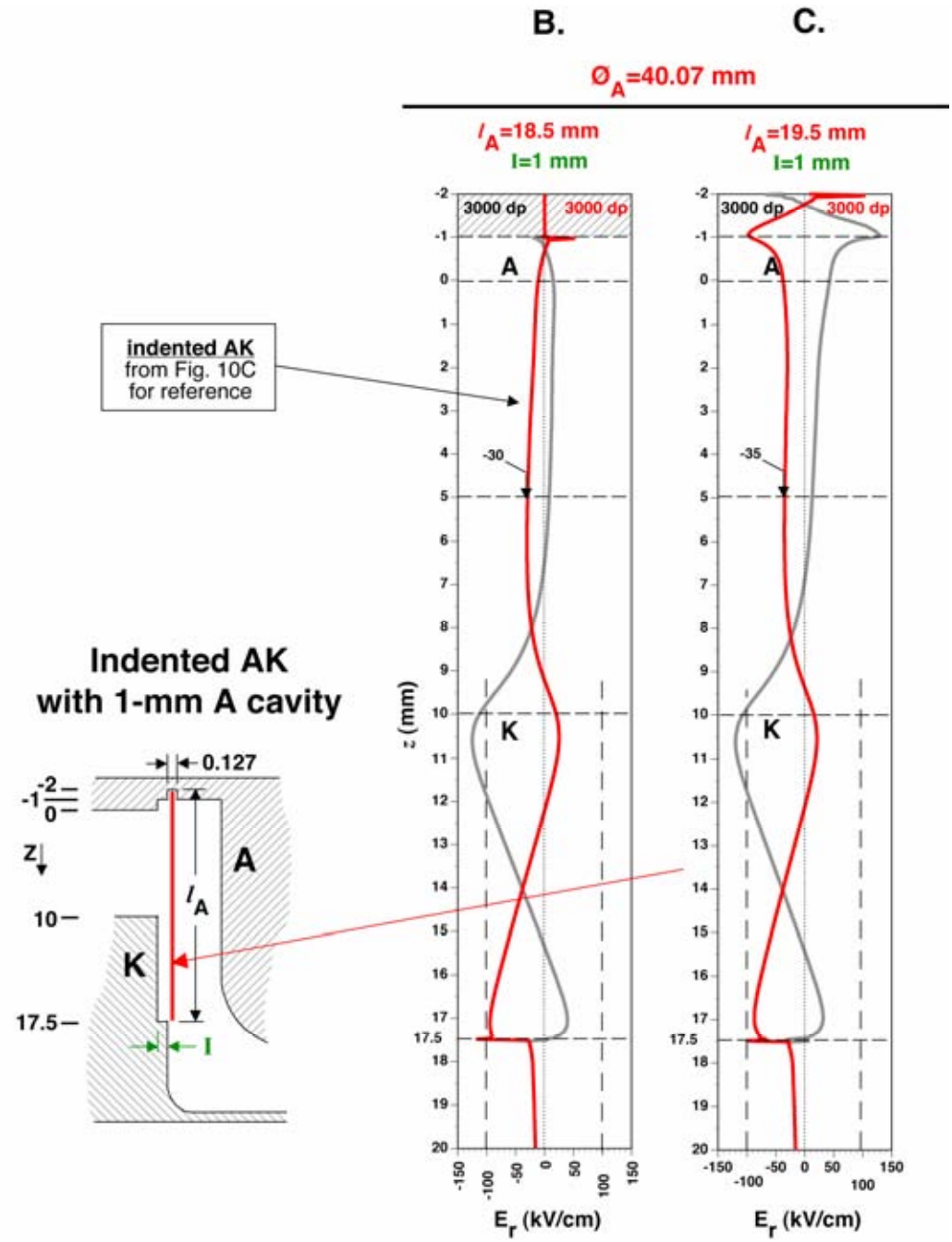

Figure 11. (A) 3D-model for deriving radial electric fields for AK 1-mm indentation (B) without and (C) with a 1-mm high, 125-μm wide anode cavity, using 35-μm wire. B is duplicated from Fig. 10C for reference. The number of data points (dp) per plot are indicated.

IX. SUMMARY

The practice of placing the current contact of the wire array at the lower region of the cathode radial surface is serendipity in reducing the negative radial electric field near the cathode of the 10-mm AK region, but bad shots from poor alignments and/or slack wires may result with the close proximity of the wire to the cathode radial surface. Indenting the cathode reduces this problem and improves the negative electric field at the anode slightly. Indenting the anode reduces the negative electric field as it reduces the anode-wire cavity depth. Both indented anode and cathode limit the negative radial electric field and aid

in clipping high negative electric field wire-end effects from the imploding plasma. With alterations in load design affecting the radial electric field parameters, the field can be verified with a 3D model aiding final design. In conclusion, the examples given show the utility of the 3D model in exploring and mitigating the negative radial electric field.

X. REFERENCES

[1] V. P. Smirnov, "Fast liners for inertial fusion", *Plasma Phys. Control. Fusion*, vol. 33, no.13, pp.1697-1714, Nov.1991.

[2] J. H. Brownell, R. L. Bowers, K. D. McLenithan, and D. L. Peterson, "Radiation environments produced by plasma z-pinch stagnation on central targets", *Phys. Plasmas*, vol. 5, no. 5, pp. 2071-2080, May 1998.

[3] T. J. Nash, M. S. Derzon, G. A. Chandler, R. Leeper, D. Fehl, J. Lash, C. Ruiz, G. Cooper, J. F. Seaman, J. McGurn, S. Lazier, J Torres, D. Jobe, T Gilliland, M. Hurst, R. Mock. P. Ryan, D. Nielsen, J. Armijo, J. McKenney, R. Hawn, and D. Hebron, "High-temperature dynamic hohlraums on the pulsed power driver Z", *Phys. Plasmas***,** vol. 6, no. 5, pp. 2023-2029, May 1999.

[4] T. W. L. Sanford, T. J. Nash, R. E. Olson, D. E. Bliss, R. W. Lemke, C. L. Olson, C. L. Ruiz, R. C. Mock, J. E. Bailey, G. A. Chandler, M. E. Cuneo, R. J. Leeper, M. K. Matzen, T. A. Mehlhorn, S. A. Slutz, W. A. Stygar, D. L. Peterson, R. E. Chrien, R. E. Watt, N. F. Roderick, G. W. Cooper, J. P. Apruzese, G. S. Sarkisov, J. P. Chittenden, and M. G. Haines, "Progress in z-pinch driven dynamic-hohlraums for high-temperature radiation-flow and ICF experiments at Sandia National Laboratories", *Plasma Phys. Control. Fusion,* vol. 46, suppl. 12B, pp. B423-B433, Dec. 2004.

[5] T.W.L. Sanford, R.E. Olson, R. L. Bowers, G. A. Chandler, M. S. Derzon, D. E. Hebron, R. J. Leeper, R. C. Mock, T. J. Nash, D. L. Peterson, L. E. Ruggles, W. W. Simpson, K. W. Struve, and R. A. Vesey, "Z-pinch-generated X-rays demonstrate potential for indirect-drive ICF experiments.", *Phys. Rev. Lett.*, vol. 83, no. 26, pp. 5511-5514, Dec. 1999.

[6] T.W.L. Sanford, R.E. Olson, R.C. Mock, C. G. Chandler, R. J. Leeper, T. J. Nash, L. E. Ruggles, W. W. Simpson, K. W. Struve, D. L. Peterson, R. L. Bowers, W. Matuska, "Dynamics of a Z-pinch X-ray source for heating inertial-confinement-fusion relevant hohlraums to 120-160 eV, *Phys. Plasmas***,** vol. 7, no. 11, pp. 4669-4682, Nov. 2000.

[7] S. A. Slutz, J. E. Bailey, G. A. Chandler, G. R. Bennett, G. Cooper, J. S. Lash, S. Lazier, P. Lake, R. W. Lemke, T. A. Mehlhorn, T. J. Nash, D. S. Nielson, J. McGurn, T. C. Moore, C. L. Ruiz, D. G. Schroen, J. Torres, W. Varnum, R. A. Vesey, "Dynamic hohlraum driven inertial fusion capsules", *Phys. Plasmas*, vol. 10, no. 5, pp. 1875-1882, May 2003.

[8] J. E. Bailey, G. A. Chandler, S. A. Slutz, I. Golovkin, P. W. Lake, J. J. MacFarlane, R. C. Mancini, T. J. Burris-Mog, G. Cooper, R. J. Leeper, T. A. Mehlhorn, T. C. Moore, T. J. Nash, D. S. Nielsen, C. L. Ruiz, D. G. Schroen, and W. A. Varnum, "Hot dense capsule-implosion cores produced by Z-pinch dynamic hohlraum radiation", *Phys. Rev. Lett*., vol. 92, no. 8, pp. 085002/1-4, Feb. 2004.

[9] C. L. Ruiz, G. W. Cooper, S. A. Slutz, J.E. Bailey, G.A. Chandler, T.J. Nash, T. A. Mehlhorn, R. J. Leeper, D. Fehl, A. J. Nelson, J. Franklin, and L. Ziegler, "Production of Thermonuclear Neutrons from Deuterium-Filled Capsule Implosions Driven by Z-Pinch Dynamic Hohlraums ", *Phys. Rev. Lett.*, vol. 93, no. 1, 015001/1-4, Jul. 2004.

[10] T. W. L. Sanford, R. W. Lemke, R. C. Mock, G. A. Chandler, R. J. Leeper, C. L. Ruiz, D. L. Peterson, R. E. Chrien, G. C. Idzorek, R. G. Watt, J. P. Chittenden, *et. al*., "Dynamics and characteristics of a 215-eV dynamic-hohlraum x-ray source on Z". *Phys. Plasmas*, vol. 9, no. 8, pp. 3573-3594, Aug. 2002.

[11] R. G. Watt, R. E. Chrien, and G. Idzorek, "Investigation of radiation in a thin Au wall using x-ray backlit imaging", *Bull. Am. Phys. Soc*., vol. 48, p. 319, Oct. 2003.

[12] T. W. L. Sanford, C. A. Jennings, G. A. Rochau, S. E. Rosenthal, G. S. Sarkisov, P. V. Sasorov, W. A. Stygar, L. F. Bennett, D. E. Bliss, J. P. Chittenden, M. E. Cuneo, M. G. Haines, R. J. Leeper, R, C. Mock, T. J. Nash, and D. L. Peterson, "Wire initiation critical for radiation symmetry in z-pinch–driven dynamic hohlraums", *Phys. Rev. Lett*., vol 98, no. 6, pp. 065003/1-4, Feb. 2007.

[13] T. W. L. Sanford, "Overview of the dynamic hohlraum x-ray source at sandia national laboratories", Sandia National Laboratories technical report SAND 2007-1734, Apr. 2007, and to be published IEEE Trans. Plasma Sci., Dec. 2007.

[14] P. V. Sasorov, Sandia National Laboratory technical presentation, 2006.

[15] Commercially available from Inegrated Engineering Software, 220-1821 Wellington Avenue, Winnipeg, Manitoba, Canada R3H 0G4, (204) 632-5636, http://integratedsoft.com.

[16] T. W. L. Sanford, R. C. Mock, J. F. Seamen, M. R. Lopez, R. G. Watt, G. C. Idzorek, and D. L. Peperson, "Wire fixturing in high wire-number z pinches critical for high radiation power and reproducibility", *Phys. Plasmas***,** vol. 12, no. 12, pp. 122701-1/8-4682, Dec. 2005.

Distribution

External:

1 Professor Jeremy Chittenden
Plasma Physics Group, Blackett Laboratories
Prince Consort Rd
South Kennsington, London
SW72BZ
UK

1 Professor Malcolm Haines
Plasma Physics Group, Blackett Laboratories
Prince Consort Rd
South Kennsington, London
SW72BZ
UK

1 Professor Sergey Lebedev
Plasma Physics Group, Blackett Laboratories
Prince Consort Rd
South Kennsington, London
SW72BZ
UK

1 Dr. Simon Bland
Imperial College London
South Kensington Campus, London
SW72AZ
UK

1 Professor David Hammer
327 Rhodes Hall
Cornell University
Ithaca, NY 14853

1 Dr. Darrell Peterson
Los Alamos National Laboratory
P.O. Box 1663
Los Alamos, NM 87545

1 Dr. Robert Watt
Los Alamos National Laboratory
P.O. Box 1663
Los Alamos, NM 87545

Internal:

2	MS 0123	D. L. Chavez, 1011
1	MS 0125	J. P. VanDevender, 12101
1	MS 0511	J. E. Maenchen, 1212
1	MS 1106	D. Ampleford, 1673
1	MS 1129	R. E. Nygren, 1658
1	MS 1152	M. L. Kiefer, 1652
1	MS 1152	L. P. Mix, 1652
1	MS 1152	T. D. Pointon, 1652
1	MS 1152	D. B. Seidel, 1652
1	MS 1152	M. Caldwell, 1653
1	MS 1159	J. W. Bryson, 1344
1	MS 1159	C. A. Coverdale, 1344
1	MS 1159	V. Harper-Slaboszewicz, 1344
1	MS 1168	C. A. Hall, 1646
1	MS 1168	D. H. McDaniel, 1650
1	MS 1168	B. M. Jones, 1673
1	MS 1168	P. D. LePell, 1673
1	MS 1178	D. D. Bloomquist, 1630
1	MS 1178	E. A. Weinbrecht, 1635
1	MS 1178	F. W. Long, 1637
1	MS 1178	D. L. Smith, 1639
1	MS 1178	G. L. Donovan, 1676
1	MS 1181	T. A. Mehlhorn, 1640
1	MS 1181	J. R. Asay, 1646
1	MS 1181	M. D. Knudson, 1646
1	MS 1181	L. C. Chhabildas, 1647
1	MS 1181	L. X. Schneider, 1650
1	MS 1186	M. P. Desjarlais, 1640
1	MS 1186	T. A. Brunner, 1641
1	MS 1186	R. B. Campbell, 1641
1	MS 1186	K. R. Cochrane, 1641
1	MS 1186	C. J. Garasi, 1641
1	MS 1186	T. A. Haill, 1641
1	MS 1186	H. L. Hanshaw, 1641
1	MS 1186	C. Jennings, 1641
1	MS 1186	R. W. Lemke, 1641
1	MS 1186	E. P. Yu, 1641
1	MS 1186	J. F. Seamen, 1670
1	MS 1186	P. J. Christenson, 1674
1	MS 1186	M. Herrmann, 1674
1	MS 1186	K. Peterson, 1674
1	MS 1186	S. E. Rosenthal, 1674
1	MS 1186	S. A. Slutz, 1674
1	MS 1186	R. A. Vesey, 1674
1	MS 1186	R. C. Mancini, 1677
1	MS 1190	M. K. Matzen, 1600
1	MS 1190	C. L. Olson, 1640

1	MS 1191	D. O. Jobe, 1670
1	MS 1191	J. L. Porter, 1670
1	MS 1191	M. A. Sweeney, 1670
1	MS 1192	M. L. Harris, 1676
1	MS 1192	J. A. Mills, 1676
1	MS 1192	G. S. Sarkisov, 1676
1	MS 1192	J. J. Seamen, 1676
1	MS 1193	K. R. Prestwich, 1645
1	MS 1193	D. C. Rovang, 1645
1	MS 1193	P. W. Spence, 1645
1	MS 1193	D. R. Welch, 1645
1	MS 1193	J. P. Corley, 1671
1	MS 1193	D. J. Johnson, 1671
1	MS 1193	J. R. Woodworth, 1671
1	MS 1193	B. W. Atherton, 1672
1	MS 1193	G. R. Bennett, 1672
1	MS 1193	J. E. Potter, 1672
1	MS 1193	M. E. Cuneo, 1673
1	MS 1193	D. L. Hanson, 1673
1	MS 1193	D. B. Sinars, 1673
1	MS 1193	G. T. Leifeste, 1675
1	MS 1193	M. R. Lopez, 1675
1	MS 1193	L. E. Ruggles, 1675
1	MS 1193	M. F. Vargas, 1675
1	MS 1193	D. F. Wenger, 1675
1	MS 1194	L. F. Bennett, 1671
1	MS 1194	D. E. Bliss, 1671
1	MS 1194	M. G. Mazarakis, 1671
1	MS 1194	M. E. Savage, 1671
1	MS 1194	K. W. Struve, 1671
1	MS 1194	E. M. Waisman, 1673
1	MS 1194	T. C. Wagoner, 1676
1	MS 1196	A. L. Carlson, 1675
1	MS 1196	D. S. Nielsen, 1675
1	MS 1196	J. E. Bailey, 1677
1	MS 1196	G. A. Chandler, 1677
1	MS 1196	G. W. Cooper, 1677
1	MS 1196	G. S. Dunham, 1677
1	MS 1196	D. L. Fehl, 1677
1	MS 1196	R. J. Leeper, 1677
20	MS 1196	R. C. Mock, 1677
1	MS 1196	T. J. Nash, 1677
1	MS 1196	R. E. Olson, 1677
1	MS 1196	G. A. Rochau, 1677
1	MS 1196	C. L. Ruiz, 1677
1	MS 1196	T. W. L. Sanford, 1677
1	MS 1196	W. A. Stygar, 1677
1	MS 1196	J. A. Torres, 1677
2	MS 9018	Central Technical Files, 8944
2	MS 0899	Technical Library, 4536